# The Effect of O-Fucosylation on the First EGF-like Domain from Human Blood Coagulation Factor VII†

Yung-Hsiang Kao,*,‡ Geoffrey F. Lee,§,|| Yang Wang,⊥ Melissa A. Starovasnik,§ Robert F. Kelley,§ Michael W. Spellman,⊥,# and Laura Lerner‡,▽

*Departments of Analytical Chemistry, Protein Engineering, and Pharmacokinetics and Metabolism, Genentech, Inc., South San Francisco, California 94080*

*Received February 1, 1999; Revised Manuscript Received March 30, 1999*

ABSTRACT: The first epidermal growth factor-like domain (EGF-1) from blood coagulation factor VII (FVII) contains two unusual O-linked glycosylation sites at Ser-52 and Ser-60. We report here a detailed study of the effect of O-fucosylation at Ser-60 on the structure of FVII EGF-1, its $Ca^{2+}$-binding affinity, and its interaction with tissue factor (TF). The in vitro fucosylation of the nonglycosylated FVII EGF-1 was achieved by using O-fucosyltransferase purified from Chinese hamster ovary cells. Distance and dihedral constraints derived from NMR data were used to determine the solution structures of both nonglycosylated and fucosylated FVII EGF-1 in the presence of $CaCl_2$. The overall structure of fucosylated FVII EGF-1 is very similar to the nonfucosylated form even for the residues near the fucosylation site. The $Ca^{2+}$ dissociation constants ($K_d$) for the nonfucosylated and fucosylated FVII EGF-1 were found to be 16.4 ± 1.8 and 8.6 ± 1.4 mM, respectively. The FVII EGF-1 domain binds to the extracellular part of TF with a low affinity ($K_d \approx 0.6$ mM), and the addition of fucose appears to have no effect on this affinity. These results indicate that the FVII EGF-1 alone cannot form a tight complex with TF and suggest that the high binding affinity of FVIIa for TF requires cooperative interaction among the four domains in FVII with TF. Although the fucose has no significant effect on the interaction between TF and the individual FVII EGF-1 domain, it may affect the interaction of full-length FVIIa with TF by influencing its $Ca^{2+}$-binding affinity.

Factor VII (FVII)[1] is a multidomain plasma glycoprotein consisting of one γ-carboxyglutamic acid (Gla)-containing domain at the N-terminus, followed by two epidermal growth factor (EGF)-like domains and one C-terminal serine protease domain. Upon vascular injury, the extrinsic pathway of blood coagulation is initiated by the activation of FVII to FVIIa and the formation of a tight complex of FVIIa with its membrane-bound cofactor, tissue factor (TF). The formation of the FVIIa:TF complex greatly enhances FVIIa activity, results in the activation of factors IX and X, and eventually leads to the production of thrombin and a fibrin clot. The crucial role of the FVIIa:TF complex in the blood coagulation cascade has led to extensive investigations of the interaction between FVIIa and TF (reviewed in ref *1*) and the designs of potent anticoagulants to block FVIIa:TF complex formation (*2*). The X-ray crystal structures of the soluble extracellular part of TF (sTF) and the FVIIa:sTF complex have been determined at 1.7 and 2.0 Å resolution, respectively (*3*−*6*), whereas the structure of FVIIa alone is not available. While all four domains of FVIIa are found to be important for its interaction with TF, mutagenesis studies on both sTF (*7*) and FVIIa (*8*, *9*) suggest that interaction with the EGF-1 domain provides a major driving force for binding of FVIIa to TF. In fact, although the size of FVII EGF-1 is small (only ∼11% of the full-length FVII in terms of sequence), the contact area between FVII EGF-1 and sTF accounts for ∼45% of the total contact area between the two molecules (*6*). Furthermore, several key residues involved in the interaction with sTF are found in EGF-1 domain (*6*, *9*). Therefore, we were interested in evaluating the binding of the isolated FVIIa EGF-1 domain to TF.

† Coordinates for the final ensemble of structures of nonfucosylated and fucosylated FVII EGF-1 have been deposited in the Brookhaven Protein Data Bank under the file names 1f7e and 1ff7.

* To whom correspondence should be addressed: Department of Analytical Chemistry, MS 62, Genentech, Inc., 1 DNA Way, South San Francisco, CA 94080.

‡ Analytical Chemistry.

§ Protein Engineering.

|| Current address: Baxter Hemoglobin Therapeutics, Process Development Department, 2545 Central Ave., Boulder, CO 80301.

⊥ Pharmacokinetics and Metabolism.

# Current address: Coulter Pharmaceutical, Inc., 550 California Ave., Suite 200, Palo Alto, CA 94326-1440.

▽ Current address: Athersys, Inc., 11000 Cedar Ave., Cleveland, OH 44106.

[1] Abbreviations: 2Q, double-quantum; CD, circular dichroism; CHO, chinese hamster ovary; DIPSI, decoupling in the presence of scalar interactions; DQF-COSY, two-dimensional double-quantum-filtered correlated spectroscopy; EGF, epidermal growth factor; FIX, blood coagulation factor IX; FVII, blood coagulation factor VII; FVIIa, activated form of blood coagulation factor VII; FX, blood coagulation factor X; FVII EGF-1, first EGF-like domain (residue 45−87) in FVII; Gla domain, γ-carboxyglutamic acid containing domain in FVII; HSQC, heteronuclear single-quantum coherence; MALDI-TOF, matrix-assisted laser desorption/ionization time-of-flight mass spectrometry; NMR, nuclear magnetic resonance; NOE, nuclear Overhauser effect; NOESY, two-dimensional nuclear Overhauser spectroscopy; rms, root-mean-square; rmsd, root-mean-square difference; TF, tissue factor; sTF, soluble extracellular part of tissue factor; TOCSY, total correlation spectroscopy; TPPI, time proportional phase incrementation; WALTZ, wide-band alternating phase low-power technique for zero residue splitting.

10.1021/bi990234z CCC: $18.00 
Published on Web 05/12/1999

The EGF-like domain is a structural motif of approximately 45 residues containing six conserved cystines which form three disulfide bonds with a 1−3, 2−4, and 5−6 pattern (*10*). This structural motif has been found in a wide range of proteins with various functions. It is believed that EGF-like domains may play an important role in mediating protein−protein interactions (*10*). The function of EGF-like domains in FVII apparently fits this role. A number of EGF-like domains, including FVII EGF-1, are known to contain a $Ca^{2+}$-binding site. The functional role of such a $Ca^{2+}$-binding site is not entirely clear. However, mutational studies of FVIIa indicated that the removal of the binding site in FVII EGF-1 resulted in the reduction of both its affinity for TF and the amidolytic activity of the protease domain (*11*, *12*). The comparison of the solution structure of $Ca^{2+}$-free FVII EGF-1 (*13*) with the $Ca^{2+}$-bound EGF-1 domain in the X-ray structure of FVIIa:sTF complex (*6*) indicated that the $Ca^{2+}$ does not cause major conformation changes in the isolated FVII EGF-1 (*13*). On the basis of the data from NMR and small-angle X-ray scattering studies, Sunnerhagen et al. (*14*) showed that the binding of $Ca^{2+}$ to FX EGF-1 alters the orientation of the Gla domain with respective to EGF-1. They proposed that the role of $Ca^{2+}$ is to rearrange and stabilize the interface between Gla and EGF-1 domains such that these domains are in the optimal conformation for the FX activity. The $Ca^{2+}$-binding site in FVII is likely to have a similar function.

Additionally, FVII EGF-1 is of particular interest because two very unusual posttranslational modifications have been observed at specific sites: an O-linked di- or trisaccharide (Xyl-Glc or Xyl-Xyl-Glc) at Ser-52 and a single O-linked fucose at Ser-60 (*15*−*17*). Little is known about these posttranslational modifications except that they appear to be restricted to EGF-like domains. The O-linked di-/trisaccharide occurs at the Ser within the sequence Cys-X-Ser-X-Pro-Cys, whereas the O-linked fucose is found at the Ser or Thr residue within the sequence Cys-X-X-Gly-Gly-Ser/Thr-Cys (*17*). The remarkable specificity of these modifications suggests that EGF-like structure may be essential for these glycosylation reactions. Glycans on glycoproteins are known to have diverse functions (*18*−*20*). It is likely that these highly specific O-glycosylation sites in FVII are of great importance for the function of FVII (*21*).

In the current study, the solution structure of the FVII EGF-1 domain was determined in the presence of $CaCl_2$. The impact of O-fucosylation at Ser-60 was evaluated by comparing the solution structures, the $Ca^{2+}$-binding affinities, and the sTF binding affinities of both fucosylated and nonfucosylated FVII EGF-1. Although the effect of O-linked di- or trisaccharide at Ser-52 may also be important (*21*), it is beyond the scope of this report. Comparison of native and nonglycosylated FVII EGF-1 is hampered by the lack of specific endoglycosidases for removing O-linked glycans quantitatively without perturbation of the protein. An alternative approach is to express the protein of interest in a bacterial system incapable of glycosylation and then to modify the protein using the appropriate glycosyltransferase and activated sugar substrate. The recent identification and purification of an O-fucosyltransferase (*22*, *23*) enabled this second approach for exploring the role of O-fucosylation in the interaction between FVII and TF.

## MATERIALS AND METHODS

*Expression of the First EGF-like Domain from Human Factor VII.* The FVII EGF-1 was expressed in *Escherichia coli* using a periplasmic secretion system as described in Wang et al. (*22*) and Wang and Spellman (*23*). The expressed domain contained 46 amino acids, comprising residues 45−87 from intact FVII in addition to a C-terminal non-FVII origin tripeptide tail, Gly-Ser-Ala. *E. coli* cells (strain 27C7) transformed with plasmid encoding the FVII EGF-1 gene were produced in a 10 L fermenter in LB medium. The uniformly $^{15}N$-labeled FVII EGF-1 was produced by expression of the same plasmid in *E. coli* K12 cells with the method of Reilly and Fairbrother (*24*).

*Purification.* The *E. coli* cell pellet was suspended and stirred in 20 mM Tris-HCl buffer, pH 8, at 4 °C for 1 h to release protein from the periplasm. The suspension was then centrifuged at 10 000 rpm for 15 min. The supernatant was filtered through an Amicon ultrafilter with a YM-10 membrane. The filtrate, containing FVII EGF-1, was concentrated by ultrafiltration using an Amicon stirred cell equipped with a YM-1 membrane. The FVII EGF-1 was purified from the retentate using a preparative scale C18 reversed-phase column (Rainin, Microsorb: 2.14 cm × 25 cm) on a BioCAD perfusion chromatography workstation (Perseptive Biosystems). The C18 column was initially equilibrated with 0.1% TFA in $H_2O$ and eluted at 10 mL/min flow rate with a linear $CH_3CN$ gradient of 4%/min for 5 min, followed by a $CH_3CN$ gradient of 1%/min for 30 min. FVII EGF-1 eluted at approximately 35% $CH_3CN$. The fractions containing FVII EGF-1 were lyophilized. If MALDI-TOF and analytical HPLC (using a C4 column on an HP 1090 system) results indicated that impurities existed, further purification was applied using a more shallow $CH_3CN$ gradient. The final yield of FVII EGF-1 was about 100 mg/L of cell culture.

*In Vitro Fucosylation.* Purified FVII EGF-1 was reconstituted in $H_2O$ to a concentration of about 3.3 mg/mL. The in vitro fucosylation was carried out by incubating 1 mg of FVII EGF-1 with 0.66 mM GDP-fucose (Boehringer Mannheim), 50 mM imidazole-HCl (pH 7.0), 50 mM $MnCl_2$ and about 4 milliunits of O-fucosyltransferase purified from CHO cells (*22*, *23*) in a total volume of 750 $\mu$L at 37 °C for at least 4 h. The reaction went to completion as confirmed by analytical HPLC using a 2.1 × 250 mm C18 reversed-phase column (Vydac), and by mass spectrometry. The fucosylated FVII EGF-1 was then purified as described above.

*Calcium-Binding Affinity of FVII EGF-1.* The $Ca^{2+}$ dissociation constant ($K_d$) of both nonfucosylated and fucosylated FVII EGF-1 was determined by $Ca^{2+}$ titration at 25 °C, pH 7.3. One-dimensional $^1H$ NMR spectra of a series of samples in $D_2O$ containing 0.22 mM (nonfucosylated) or 0.21 mM (fucosylated) FVII EGF-1, 20 mM Tris-$d_{11}$, and variable concentrations (0−500 mM) of $CaCl_2$ were recorded. FVII EGF-1 concentrations were determined with amino acid composition analysis. The ionic strength was maintained at 150 mM by adding NaCl for the samples with a $CaCl_2$ concentration lower than 50 mM. The change in chemical shifts (in hertz) of several signals, including $C^{\gamma}H_2$ of Pro-54 and $H^{\alpha/\delta}$ of Tyr-68, were plotted against the total concentration of $Ca^{2+}$ in the sample. The $Ca^{2+}$ dissociation constant was derived from the $Ca^{2+}$ titration curve with a fitting

procedure essentially the same as described by Persson et al. (*25*).

*Tissue Factor Binding Assay.* The apparent binding affinities of FVII EGF-1 domains for sTF were evaluated from the inhibition of sTF stimulated FVIIa amidolytic activity. Concentrations of stock solutions of EGF-1 domains were determined by quantitative amino acid analysis. sTF at a concentration of 50 nM was incubated with 50 nM FVIIa and a varied concentration of fucosylated or nonfucosylated EGF-1 domain in a solution containing 0.2 M Hepes, pH 7.5, 0.1 M NaCl, 50 mM $CaCl_2$, and 0.01% Tween-20. After a 1 h incubation at ambient temperature, the FVIIa substrate chromozym t-PA (*N*-methylsulfonyl-D-phenyl-L-glycyl-L-arginine-*p*-nitroanilide acetate; Boehringer Mannheim) was added to a final concentration of 0.5 mM, and the change in absorbance at 405 nm was measured using a plate reader (EAR340AT, SLT-Lab Instruments, Austria) at ambient temperature. Rates of substrate hydrolysis were determined by linear regression using software supplied by the manufacturer. Fractional rates were calculated by dividing these rates by the value measured for no added EGF-1 domain. The concentration of EGF-1 giving 50% inhibition ($IC_{50}$) was determined using a nonlinear regression analysis as described in Kelley et al. (*26*).

In addition to the binding assay described above, the interaction between the isolated FVII EGF-1 domain and sTF was also examined by recording $^1$H-$^{15}$N HSQC spectra of $^{15}$N-labeled FVII EGF-1 in the presence of varying concentrations of sTF. Six samples of both nonfucosylated and fucosylated $^{15}$N-labeled FVII EGF-1 (0.25 mM) were incubated with 0, 0.05, 0.15, 0.3, 0.6, and 1.0 mM of sTF in a buffer at pH 7.0 containing 20 mM Tris-$d_{11}$, 100 mM NaCl, and 100 mM $CaCl_2$. $^1$H-$^{15}$N HSQC spectra of these samples were recorded using the method and parameters as described below.

*NMR Samples.* NMR samples were prepared in a 90% $H_2O$/10% $D_2O$ solution containing 20 mM sodium acetate-$d_3$ (Isotec, Inc.), pH 5.5, 100 mM NaCl, 100 mM $CaCl_2$, and 0.01% $NaN_3$ for both fucosylated and nonfucosylated FVII EGF-1. Since the $Ca^{2+}$ titration experiments suggested a low $Ca^{2+}$-binding affinity of the FVII EGF-1 domain (see Results and Discussion), a high concentration of $CaCl_2$ (100 mM) was therefore used in all NMR samples to minimize the population of $Ca^{2+}$-free FVII EGF-1. Final protein concentrations were 1.8 and 1.1 mM for nonfucosylated and fucosylated samples, respectively. $^{15}$N-labeled FVII EGF-1 samples were prepared in the same buffer; final concentrations were 2.4 mM and 0.8 mM for nonfucosylated and fucosylated FVII EGF-1, respectively. Samples for amide hydrogen exchange experiments were prepared by lyophilizing $^{15}$N labeled FVII EGF-1 from $H_2O$ (after extensive dialysis in $H_2O$) and reconstituting the samples in the 100% $D_2O$ solution containing 20 mM sodium acetate-$d_3$, pH 5.5, 100 mM NaCl, 100 mM $CaCl_2$, and 0.01% $NaN_3$. Sample volumes were 110 $\mu$L or 120 $\mu$L in 3 mm Shigemi microtubes (Shigemi, Inc.) for all NMR experiments except the amide hydrogen exchange measurements.

*NMR Experiments.* All NMR experiments were performed at 25 °C on a Varian INOVA 500 MHz spectrometer equipped with a Nalorac 3 or 5 mm triple resonance pulsed-field gradient probes. All data were processed with the program FELIX (Molecular Simulation, Inc.) on an SGI Indigo2 work station (Silicon Graphics, Inc.). The following two-dimensional spectra were recorded using standard pulse sequences: DQF-COSY (*27*), 2Q (*28, 29*), TOCSY (*30, 31*), and NOESY (*32,33*). The double gradient echo sequence of Hwang and Shaka (*34*) was included in TOCSY and NOESY experiments for water suppression. TOCSY spectra were recorded using a 50 ms DIPSI-2rc sequence (*35*) for isotropic mixing. NOESY spectra were collected using 50, 100, and 150 ms mixing times. Either TPPI (*36, 37*) or TPPI-States (*38*) was employed for quadrature detection with 512 points in the $t_1$ dimension for all proton data. DQF-COSY experiments were performed using 2048 complex points in the $t_2$ dimension with a spectral width of 6250 Hz in both $F_1$ and $F_2$ dimensions. 2*Q* data were collected with an excitation period of 40 ms and spectral widths of 12 500 and 6250 Hz in the $F_1$ and $F_2$ dimensions, respectively. NOESY and TOCSY spectra were acquired with a spectral width of 12 500 Hz in the $F_2$ dimension using 4096 complex points and a 6250 Hz spectral width in the $F_1$ dimension. Zero-filling was used in the $t_2$ dimension to give a final matrix of 2048 × 2048 points for all 2D spectra.

2D $^1$H-$^{15}$N HSQC, 3D $^1$H-$^{15}$N NOESY-HSQC, and 3D $^1$H-$^{15}$N TOCSY-HSQC spectra were recorded with pulse sequences employing a selective "water flip back" pulse to minimize water saturation for these heteronuclear experiments (*39, 40*). These experiments are based on the sensitivity-enhanced gradient approach (*41, 42*) which requires postacquisition processing to yield pure absorptive spectra by adding and subtracting the N- and P-type data recorded separately for each time increment, following a 90° zero-order phase correction for one of the two resulting data sets. This process was built in as part of the Felix macro programs for the Fourier transform of all the sensitivity-enhanced data. Quadrature detection in the indirectly acquired dimensions was achieved with the TPPI-States method for all heteronuclear experiments. For $^1$H-$^{15}$N HSQC experiments, a WALTZ-16 sequence (*43*) was used for $^{15}$N decoupling during acquisition, whereas GARP-1 (*44*) was used for the 3D $^1$H-$^{15}$N NOESY-HSQC and TOCSY-HSQC experiments. $^1$H-$^{15}$N HSQC spectra were recorded with a spectral width of 8000 Hz over 2048 complex points in the $^1$H dimension and 2000 Hz over 128 complex points in the $^{15}$N dimension. 3D $^1$H-$^{15}$N NOESY-HSQC spectra were recorded with a mixing time of 150 ms. An isotropic mixing time of 30 ms was achieved with a DIPSI-2rc spin-locking sequence in 3D $^1$H-$^{15}$N TOCSY-HSQC experiments. The 3D data were collected in matrixes of 128 complex ($^1$H, $t_1$) × 32 complex ($^{15}$N, $t_2$) × 1024 complex ($^1$H, $t_3$) points with spectral widths of 6250 Hz ($F_1$), 1500 Hz ($F_2$), and 6250 Hz ($F_3$). After zero-filling, final spectra were stored in matrixes of 512 ($F_1$) × 64 ($F_2$) × 1024 ($F_3$) points.

To estimate side-chain $\chi_1$ dihedral angles, 3D constant-time HNHB spectra (*45*) were recorded in data matrixes of 64 complex ($^1$H, $t_1$) × 32 complex ($^{15}$N, $t_2$) × 1024 complex ($^1$H, $t_3$) points with spectral widths of 6250 Hz ($F_1$), 1500 Hz ($F_2$), and 6250 Hz ($F_3$). $^{15}$N decoupling during acquisition was achieved using a WALTZ-16 sequence. Final spectra were stored in matrixes of 256 ($F_1$) × 128 ($F_2$) × 1024 ($F_3$) points. $^3J_{HN-H\alpha}$ coupling constants were determined from DQF-COSY spectra and from 3D HNHA experiments (*46*). HNHA spectra were recorded with the same spectral widths, decoupling sequence, and data matrix size as used in 3D

HNHB experiments. For clearly resolved $H^N-H^\alpha$ cross-peaks in DQF-COSY, the $^3J_{HN-H\alpha}$ coupling constants were consistent with the values obtained from HNHA experiments. Since several signals were bleached out by the presaturation pulse and several others were not well resolved in the DQF-COSY experiment, the values obtained from HNHA were therefore used for estimating backbone dihedral angels.

*Interproton Distance and Dihedral Angle Constraints.* The NOE cross-peaks observed in 2D NOESY spectra with a mixing time of 150 ms were classified as strong, medium, weak, or very weak corresponding to upper distance bounds of 2.7, 3.3, 5.0, and 6.0 Å, respectively. The lower bound for all NOE constraints was set to 1.8 Å. For overlapped cross-peaks, the upper bounds were increased by one or more categories qualitatively depending on the extent of overlap to ensure that the interproton distances were not over-constrained. The upper bound for methyl protons was increased by 0.5 Å (*47*). For methyl protons, nonstereospecifically assigned methylene protons, and aromatic side-chain protons, $<r^{-6}>$ averaging was applied.

Amide protons protected from exchange with solvent were identified by amide hydrogen/deuterium exchange experiments using a series of HSQC spectra recorded after reconstituting the protein in deuterated buffer. These protected amide protons are presumably either involved in hydrogen bonds or buried in the interior of the protein. When a hydrogen bond acceptor could be clearly identified in the initial structures for a protected amide proton, two distance constraints ($d_{NH-O} = 1.8-2.2$ Å and $d_{N-O} = 1.8-3.3$ Å) were then included in the refinement stage of structure calculation for each hydrogen bond.

The backbone $\phi$ angle constraints were set to be $-90 > \phi > -150$ for $^3J_{HN-H\alpha} > 8$ Hz and $-50 > \phi > -80$ for $^3J_{HN-H\alpha} < 5$ Hz. Stereospecific assignments for $\beta$ methylene protons and side-chain $\chi_1$ dihedral angle constraints were obtained on the basis of data from 3D TOCSY-HSQC (with 30 ms isotropic mixing time), 3D HNHB, and NOESY (50 ms mixing time) experiments. The $\chi_1$ torsion angles were restrained to $\pm 20°$ of the preferred $\chi_1$ rotamer ($-60°$, $180°$, or $+60°$) (*48*).

*Structural Calculations.* The hybrid distance geometry-simulated annealing method of Nilges et al. (*49*) was employed for the structure calculation. One hundred initial structures were obtained by embedding the distances into Cartesian coordinates and by optimizing the embedded structures with a simulated annealing protocol. These structures were then subject to several rounds of restrained dynamical simulated annealing refinement and restrained energy minimization to yield final structures. The carbohydrate parameters modified from a standard force field for crystallography refinement in X-PLOR were taken from Fletcher et al. (*50*). The $\alpha 1 \rightarrow$ O−Ser linkage for the O-linked fucose was added to the topology file in the structure calculation of fucosylated FVII EGF-1. Six additional improper angles were defined in the parameter set to enforce a $^1C_4$ conformation for the fucose. All structure calculations were performed using the program X-PLOR 3.851 (*51*). An iterative structure refinement approach (*48*) was taken to ensure that any incorrect NOE constraints were either excluded or corrected and that the upper bounds on constraints were not underestimated. The initial structure calculation was carried out using distance constraints derived from NOESY data only. Backbone $\phi$ angle constraints, side-chain $\chi 1$ dihedral angles constraints, and hydrogen bond constraints were included sequentially at separate stages of structure refinement. The 20 lowest energy structures were chosen to represent the solution structures of the fucosylated and nonfucosylated FVII EGF-1.

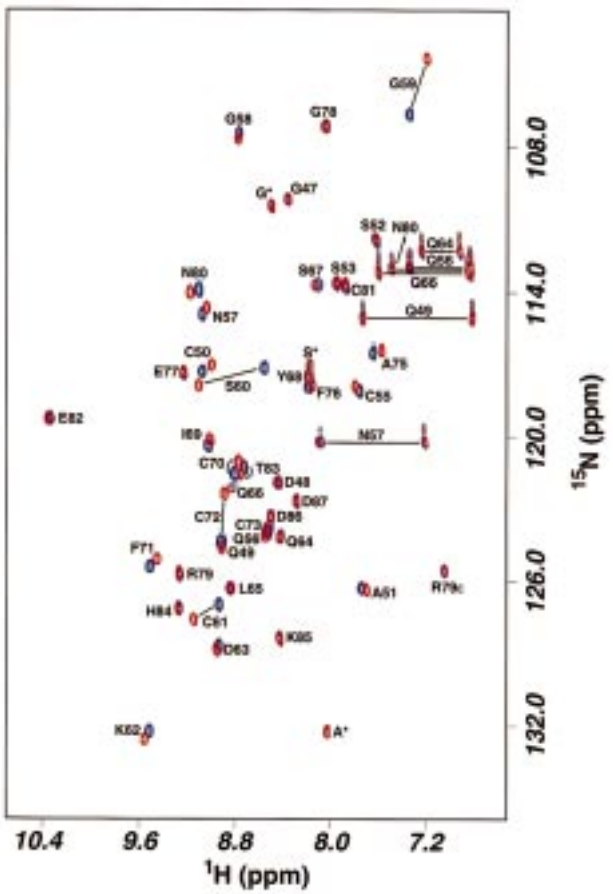


FIGURE 1: Overlay of $^1$H-$^{15}$N HSQC spectra of nonfucosylated (red) and fucosylated (blue) $^{15}$N-labeled FVII EGF-1 recorded at 298 K and pH 5.5 in the presence of 100 mM NaCl and 100 mM $CaCl_2$. Several residues showing a large $^1$H or $^{15}$N chemical shift change upon fucosylation are indicated by solid lines. Side-chain amide signals are linked by horizontal lines. The cross-peak for $N^\epsilon H$ of Arg-79 (labeled as R79$\epsilon$) is folded in from 86.1 ppm in the $^{15}$N dimension. The cross-peaks labeled with an asterisk are the three non-FVII origin tripeptide (Gly-Ser-Ala) tail at the C-terminus.

## RESULTS AND DISCUSSION

*NMR Measurements and Assignments.* As FVII EGF-1 is a relatively small domain (46 residues), all proton resonances except a few N- and C-terminal residues could be identified and sequence-specifically assigned with conventional 2D NMR methods (*52*). The data from proton-detected $^{15}$N heteronuclear experiments (i.e., $^1$H-$^{15}$N HSQC, $^1$H-$^{15}$N TOCSY-HSQC, and $^1$H-$^{15}$N NOESY-HSQC) were used primarily to assign $^{15}$N resonance frequencies and to confirm the proton resonance assignments. The 3D data were used to resolve some ambiguities in 2D NOESY spectra. As a comparison, Figure 1 presents the $^1$H-$^{15}$N HSQC spectra of fucosylated (blue) and nonfucosylated (red) FVII EGF-1 collected at 298 K and pH 5.5 in the presence of 100 mM NaCl and 100 mM $CaCl_2$. The largest chemical shift difference resulting from fucosylation occurs at Ser-60, the fucosylation site, and a few residues flanking Ser-60 (e.g.,

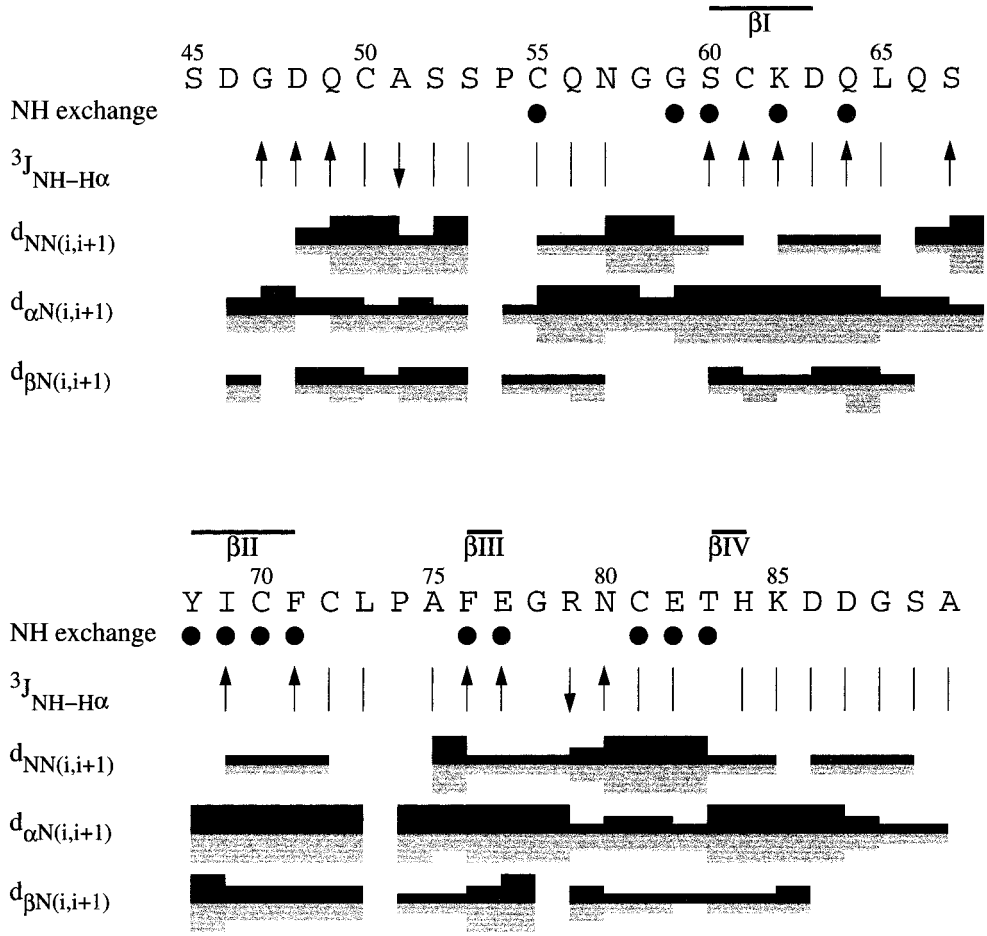


FIGURE 2: Summary of sequential NOE connectivities, amide hydrogen exchange, and $H^N$-$H^\alpha$ coupling constants for FVII EGF-1. The sequential NOEs are indicated by black (nonfucosylated) and gray (fucosylated) shaded bars; the thickness of the bars represents the relative intensity of the sequential NOE connectivities. The amide hydrogens that were still observed in the HSQC spectrum 7 h after dissolving in $D_2O$ are indicated by filled circles. The values of $^3J_{HN-H\alpha}$ coupling constants were summarized using the following symbols: (↓) $^3J_{HN-H\alpha} < 5$ Hz; (|) 5 Hz $\leq {}^3J_{HN-H\alpha} \leq 8$ Hz; (↑) $^3J_{HN-H\alpha} > 8$ Hz. The protected amide hydrogens and the $^3J_{HN-H\alpha}$ coupling constants are essentially the same in both nonfucosylated and fucosylated FVII EGF-1.

residues 57−59 and 61−63). There are also significant spectral differences observed for residues that are far from the fucosylation site in sequence; for example, residues 49−51, 70−72, 75, 80, and 83. The changes at residues 49−51 are intriguing because they are close to the second glycosylation site, Ser-52, raising the possibility of communication between the two O-linked sites. In addition, some of these affected residues (i.e., Gln-49, Asp-63) are found to be directly involved in the $Ca^{2+}$-binding site in the X-ray structure of FVIIa:sTF complex (*6*), suggesting that the fucose could influence the $Ca^{2+}$-binding site structure and/or affinity in FVII EGF-1. In both nonfucosylated and fucosylated FVII EGF-1, the amide peak for Gln-66 is significantly broadened, presumably as a result of an exchange process occurring at an intermediate rate on the NMR time scale.

A figure comparing the 3D composite HSQC-NOESY strip plots of nonfucosylated and fucosylated FVII EGF-1 for residues near Ser-60 is provided in Supporting Information. Sequential NOE connectivities are summarized in Figure 2. Overall, the observed NOE patterns for nonfucosylated and fucosylated FVII EGF-1 are very similar. Complete $^{15}N$ and $^1H$ chemical shifts for both nonfucosylated and fucosylated FVII EGF-1 are listed in Supporting Information Table S1. Stereospecific assignments were made for 13 of 24 residues with nondegenerate $\beta$-methylene protons for both fucosylated and nonfucosylated forms based on the analyses of HNHB, 3D $^1H$-$^{15}N$ HSQC-TOCSY, and short mixing time NOESY data. These assignments are also included in Table S1. The $\chi_1$ dihedral angle constraints for these residues were used in the structure calculation.

From 3D HNHA experiments, 41 $^3J_{HN-H\alpha}$ coupling constants were determined for both nonfucosylated and fucosylated FVII EGF-1 (Figure 2). The values are very similar in both cases, suggesting that the backbone structure is not altered significantly by fucosylation. There are two residues found to have $^3J_{HN-H\alpha} < 5$ Hz, and 13 have $^3J_{HN-H\alpha} > 8$ Hz. A total of 14 backbone amide protons were found to be protected against exchange with solvent as determined by hydrogen/deuterium exchange experiments using a series of HSQC experiments. Again, the results from hydrogen exchange experiments are virtually the same for nonfucosylated and fucosylated FVII EGF-1, indicating that fucosylation of FVII EGF-1 does not change the pattern of hydrogen bonds and/or the solvent accessibility of these amides. The hydrogen exchange data are also summarized in Figure 2.

*Structure Calculation and Final Structures.* A total of 20 structures with the lowest energies after the restrained molecular dynamics refinement were selected to represent

Table 1: Statistics for FVII EGF-1 NMR Structures

| | final structures[a] nonfucosylated | minimized mean[b] nonfucosylated | final structures[a] fucosylated | minimized mean[b] fucosylated |
|---|---|---|---|---|
| | rms deviation from experimental constraints | | | |
| distant constraints (Å)[c] | 0.005 ± 0.001 | 0.006 | 0.005 ± 0.001 | 0.004 |
| dihedral constraints (deg)[d] | 0.095 ± 0.038 | 0.072 | 0.118 ± 0.028 | 0.050 |
| no. of violations | | | | |
| distance violations > 0.01 Å | 34 ± 4 | 40 | 32 ± 5 | 27 |
| maximum (Å) | 0.07 ± 0.03 | 0.10 | 0.08 ± 0.03 | 0.07 |
| dihedral violations > 0.1 deg | 4 ± 2 | 3 | 7 ± 1 | 2 |
| maximum (deg) | 0.62 ± 0.20 | 0.5 | 0.75 ± 0.21 | 0.4 |
| | rms deviation from idealized covalent geometry[e] | | | |
| bonds (Å) | 0.0028 ± 0.0001 | 0.0029 | 0.0029 ± 0.0001 | 0.0028 |
| angles (deg) | 0.55 ± 0.01 | 0.56 | 0.56 ± 0.01 | 0.55 |
| impropers (deg) | 0.37 ± 0.01 | 0.36 | 0.41 ± 0.01 | 0.41 |
| | rms deviations from the mean structure (Å)[f] | | | |
| backbone (N−C−C$^a$) | | | | |
| residues 47−84 | 0.61 ± 0.10 | | 0.72 ± 0.12 | |
| $\beta$-sheets[g] | 0.50 ± 0.11 | | 0.49 ± 0.09 | |
| all residues | 2.33 ± 0.49 | | 2.21 ± 0.45 | |
| all heavy atoms | | | | |
| residues 47−84 | 1.02 ± 0.11 | | 1.13 ± 0.12 | |
| $\beta$-sheets[g] | 0.84 ± 0.11 | | 0.95 ± 0.12 | |
| all residues | 2.41 ± 0.41 | | 2.28 ± 0.35 | |

[a] The 20 final structures; mean values and standard deviations are shown. [b]Energy-minimized mean structure. The mean structure was obtained by taking the mathematical average of the 20 final structures aligned with the backbone atoms (N−C−C$^a$) of residues 47−84. [c] A total of 539 and 552 distance constraints were included in the structure calculations for nonfucosylated and fucosylated FVII EGF-1, respectively: 110 (nonfucosylated) and 113 (fucosylated) were sequential; 81 (nonfucosylated) and 71 (fucosylated) were medium-range ($1 < |i - j| < 5$); 159 (nonfucosylated) and 166 (fucosylated) were long range ($|i - j| \geq 5$); 189 (nonfucosylated) and 202 (fucosylated) were intraresidue; 14 distant constraints for 7 H-bonds were included for both forms of FVII EGF-1. [d] A total of 15 backbone $\phi$ angle constraints and 13 side-chain $\chi_1$ angle constraints were used in the structure calculation. [e] Idealized covalent geometry is defined by the force field for NMR structure calculation in X-PLOR. [f] The rms differences of the atomic positions were calculated for the 20 final structures against the mean structure. [g] The $\beta$ sheets are formed by the following residues: 60−65 and 68−71 for sheet I (major); 76−77 and 83−84 for sheet II (minor).

the solution structures for both nonfucosylated and fucosylated FVII EGF-1. The experimental constraints used in the structure calculation and the statistics for the final ensemble of structures are summarized in Table 1. These final structures have no distance constraint violations greater than 0.12 Å (nonfucosylated) and 0.17 Å (fucosylated) and no dihedral constraint violations greater than 1.2° (nonfucosylated) and 1.3° (fucosylated). Ramachandran plots generated with the program PROCHECK-NMR (*53*) for the 20 final structures indicate that 63.3% of the $\phi,\psi$ angles of resides 47−64 and 67−84 in both nonfucosylated and fucosylated FVII EGF-1 are within the most favored regions; 36.7% (nonfucosylated) and 36.0% (fucosylated) are within the additionally allowed regions; and 0.7% (fucosylated) are within the generously allowed regions.

The superposition of the 20 final structures is shown in Figure 3. These structures are superimposed by minimizing the difference for the backbone atoms of residues between 47 and 84. The backbone atom rmsd from the mathematical average of the 20 structures for these residues (47−84) is 0.61 Å for nonfucosylated FVII EGF-1 and 0.72 Å for fucosylated form. In the well-defined $\beta$-sheet regions, the rmsd values are 0.50 and 0.49 Å for nonfucosylated and fucosylated FVII EGF-1, respectively (Table 1). Of the three disulfide bonds, the first (Cys-50−Cys-61) is poorly defined presumably as a result of insufficient NOE constraints. Although the second and third disulfide bonds are fairly ordered, they both diverge into two subgroups corresponding to a left- and right-handed disulfide conformation. As a result of the two possible conformations for the disulfide bond Cys-72−Cys-81, the backbone structure between residue 71 and 75 also diverges into two subsets.

Structure analysis using the program PROCHECK-NMR (*53*) indicated that both nonfucosylated and fucosylated FVII EGF-1 structures consist of two antiparallel two-stranded $\beta$ sheets: the first contains residues 60−63 and 68−71, the second contains residues 76−77 and 83−84 (Figure 4). This structural motif is characteristic of an EGF-like structure (*10*) and identical to the FVII EGF-1 domain in the X-ray structure of FVIIa in complex with sTF (*6*), indicating that the fucosylation does not significantly affect the structure of the EGF-like motif. While the FVII EGF-1 structure is unaffected by the fucose, chemical shift perturbations were observed for several residues (Figure 1). Among these, a few are spatially close to the fucose (e.g., Phe-71 and Cye-72), whereas others are somewhat at a distance from the fucosylation site (e.g., Asn-80, Thr-83, Cys-50, and Ala-51) (Figure 4). Presumably, slight rearrangement of the aromatic ring of Phe-71 upon fucosylation could result in ring current shift changes on neighboring residues. In addition, the disulfide bridges may transmit small perturbations to sites that are remote from the fucose. However, the precision of the NMR structures does not allow for a clear description of these minor structural effects.

The backbone structures of the two short sheets are very well-defined as indicated by the superimposed structure ensemble (Figure 3) with low backbone rmsd values and angular order parameters (*54*) in these regions (Figure 5). However, the relative orientation of the two $\beta$-sheets is less well-defined. When the ensemble of final structures is superimposed on either one of the two $\beta$-sheets, the other sheet spans across a much larger space (Figure 6). This type of disorder in the ensemble may arise from mobility due to insufficient stabilizing interactions between the two subdo-

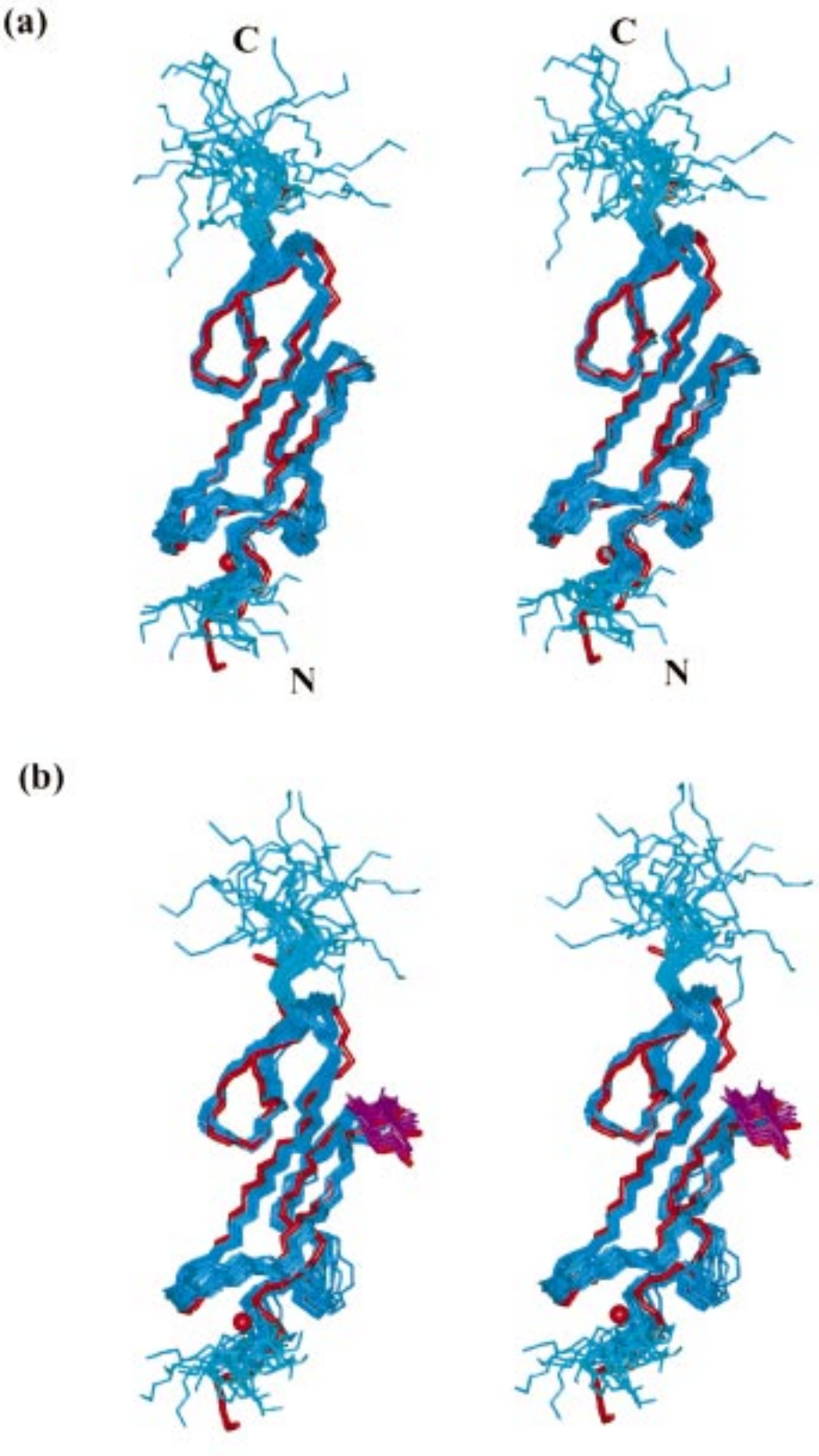


FIGURE 3: Stereoviews of the superposition of the 20 final structures for nonfucosylated (a) and fucosylated (b) FVII EGF-1. These structures are superimposed by minimizing the difference for the backbone atoms of residues 47−84, which are colored in darker blue. The fucose in the fucosylated FVII EGF-1 is shown in purple. As a comparison, the backbone structure of FVII EGF-1 (shown in red) taken from the X-ray structure of FVIIa:sTF complex (*6*) is superimposed with the 20 final structures. The red sphere indicates the position of $Ca^{2+}$ in the X-ray structure.

mains and/or the lack of inter-subdomain NOEs. It has been suggested that there may exist a hinge-bending motion between the two $\beta$-sheets in other EGF-like domains (*55*, *56*). Further $^{15}N$ relaxation studies are required to determine

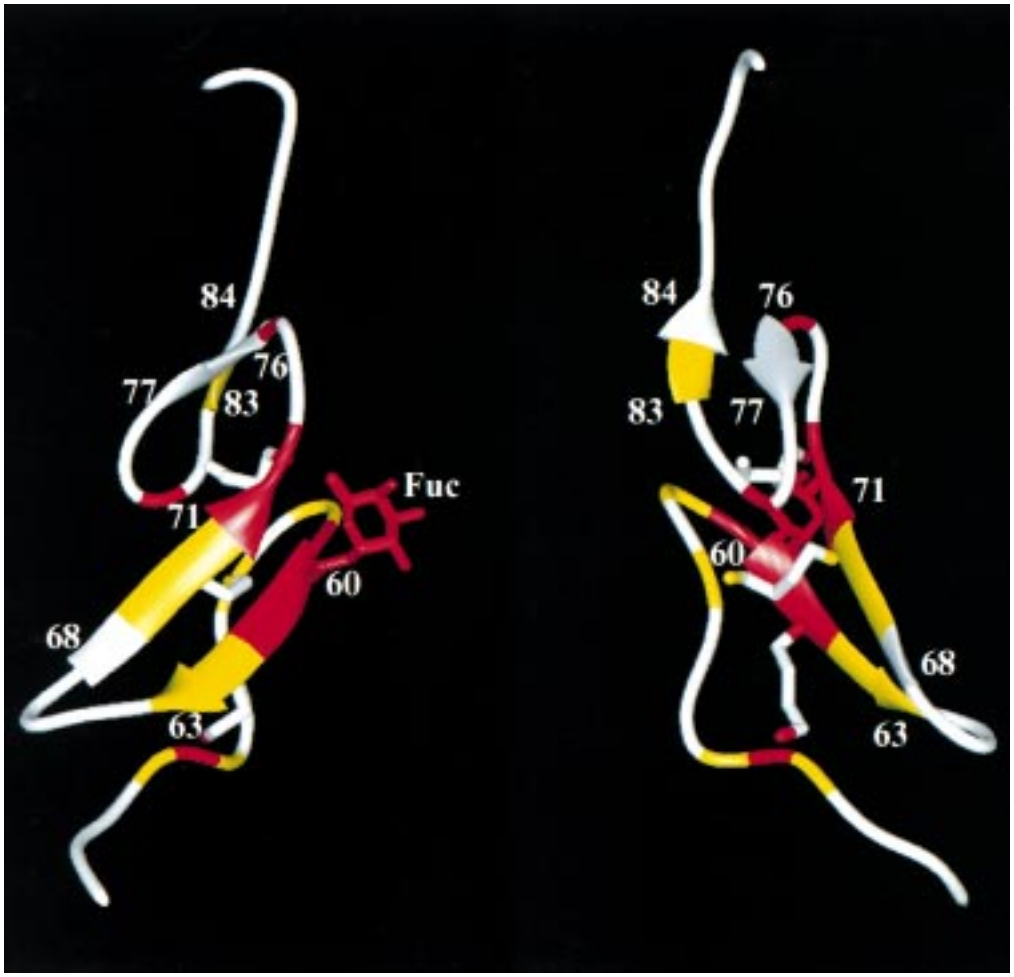


FIGURE 4: The schematic representation of the energy-minimized mean structure of fucosylated FVII EGF-1 showing the secondary structure in two different views. Residues are numbered at the start and the end of each $\beta$-stand. The fucose, Ser-60 and the three disulfide bridges (Cys-50−Cys-61, Cys-55−Cys-70, and Cys-72−Cys-81) are shown. Highlighted in red and yellow are those residues whose $^1$H-$^{15}$N cross-peaks in the HSQC spectra are affected upon fucosylation. Red ($^1$H-$^{15}$N cross-peaks in the nonfucosylated and the fucosylated spectra are completely separate): residues 50, 59, 60, 61, 71, 72, 75, and 80; Yellow ($^1$H-$^{15}$N cross-peaks in the nonfucosylated and the fucosylated spectra are shifted but partially overlap): residues 49, 51, 55, 57, 58, 62, 63, 69, 70, and 83.

if similar motion is present in FVII EGF-1.

In addition to the two $\beta$-sheets, three turn structures can be readily identified in the final structures. The backbone structure of residues 56−59 is consistent with a type I′ turn (*57*, *58*). The fucosylation at Ser-60 has no effect on the backbone structure of this turn (Figure 7). Residues 73−76 between the two $\beta$-sheets adopt a twisted type I $\beta$-turn structure. Residues 78−81, which connect $\beta$-strands III and IV of the second sheet, form a type I $\beta$-turn. As expected for these $\beta$-turn structures, hydrogen bonds Gln-56 O:Gly-59 $H^N$, Leu-73 O:Phe-76 $H^N$, Gly-78 O:Cys-81 $H^N$ were found in >75% of the initial structures calculated without using the distance constraints for hydrogen bonds. These hydrogen bonds are consistent with results from the hydrogen/deuterium exchange experiments: the amide protons for residues 59, 76, and 81 are found to be protected against the exchange with solvent.

The type I′ $\beta$-turn of residues 56−59 is perhaps the most intriguing part of the FVII EGF-1 structure (Figure 7). This turn is within the putative consensus sequence, CXXGG**S**/**T**C, identified for the fucosylation site in several EGF-like domains (*17*). In the absence of $GDP^-$fucose, the FVII EGF-1 appears to bind the O-fucosyltransferase tightly (*23*). It is possible that this $\beta$-turn structure is essential for recognition by the O-fucosyltransferase. Additionally, the overall fold of FVII EGF-1 may also be critical in terms of the specificity and reactivity of the O-fucosyltransferase. Wang and Spellman (*23*) reported that replacing the two Gly residues in the putative consensus sequence for fucosylation (CXXGGS/TC) with alanine, either individually or jointly, appears to create multiple species of FVII EGF-1 with different disulfide pairing based on the HPLC and LC/MS analysis; however, only the molecules with the correct disulfide pairing can be fucosylated. These results suggest that the EGF-like structure and correct disulfide pairing are essential for FVII EGF-1 to be O-fucosylated. Although the two Gly residues are not absolutely required for an EGF-like domain, they occur in other EGF-like domains with a remarkably high frequency. Apparently, only the correct disulfide pairing can provide the type I′ $\beta$-turn structure of residues 56−59 required for fucosylation. However, the interaction between the O-fucosyltransferase and its substrate (FVII EGF-1) is likely to involve residues outside of this turn. Further investigation is underway in our laboratory to characterize the binding interface between FVII EGF-1 and the O-fucosyltransferase.

The fucosylation occurs at Ser-60, which is the first residue of strand I and located between the second and third cysteine.

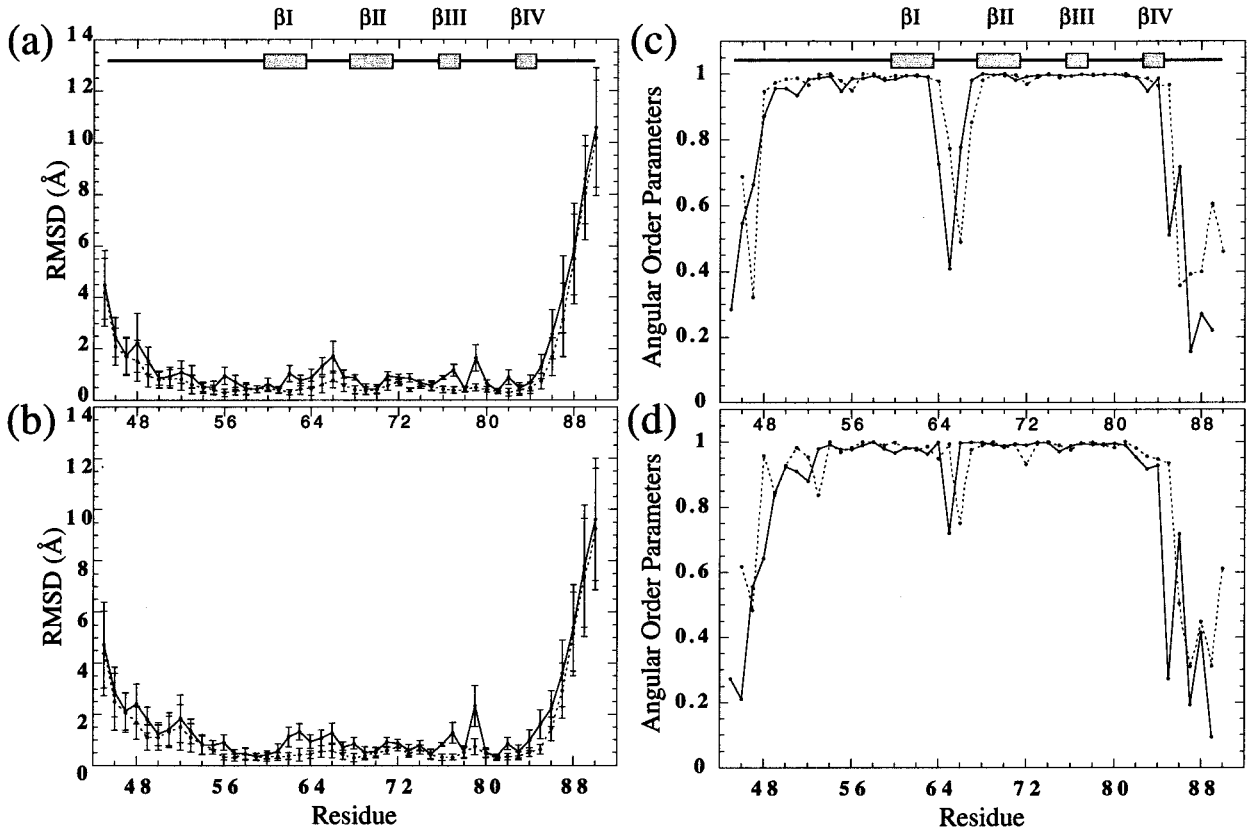


FIGURE 5: Plots of atomic rms difference from the mean structure (average ± SD) vs residue number for backbone non-hydrogen atoms (dotted) and all non-hydrogen (solid): (a) nonfucosylated and (b) fucosylated FVII EGF-1. Plots of angular order parameters vs residues for backbone $\phi$ (dotted) and $\psi$ (solid) dihedral angles: (c) nonfucosylated and (d) fucosylated FVII EGF-1. The regions corresponding to the four $\beta$-strands are indicated in panels a and c.

Ser-60 is fully exposed in the nonfucosylated FVII EGF-1 structure. Only a few NOEs were observed between the fucose and FVII EGF-1 domain: Phe-71 $H^{\beta}$s and Cys-72 $H^{N}$ to the methyl group of fucose and Leu-73 $H^{\gamma}$ and both $C^{\delta}H_3$ groups to H4 of fucose. However, these long-range NOEs are sufficient to give rise to a well-defined orientation for the sugar. Both fucose and Ser-60 are relatively well-defined in the structural ensemble of the fucosylated FVII EGF-1. The methyl group of the fucose is pointing toward the backbone of Phe-71 and Cys-72. The orientation of fucose in the NMR structure is similar to that observed in the X-ray structure of full-length FVIIa complexed with sTF (*6*), suggesting that neither the complexation with sTF nor the removal of other domains affects the position of the sugar.

In contrast to the well-defined sheet and turn structures, the N-terminal residues 45−46 and C-terminal residues 85−86 with the Gly-Ser-Ala tail are completely disordered in the ensemble of structures for both nonfucosylated and fucosylated FVII EGF-1. In addition, the loop connecting the $\beta$-strands I and II in the first sheet (residues 64−67) is less well-defined (Figures 3 and 5). N-terminal residues 47−52 are also slightly disordered. The disorder in these regions may arise from higher mobility or insufficient experimental constraints. To distinguish these two situations and to characterize the conformational dynamics, a complete analysis of backbone $^{15}N$ relaxation data is required. Preliminary data from the backbone $^{15}N$-$^{1}H$ heteronuclear NOE measurements for the nonfucosylated FVII EGF-1 indicate that the possible flexible regions, where $^{15}N$-$^{1}H$ heteronuclear NOE values are small or negative, are limited to the first two residues at the N-terminus, the last five residues at the C-terminus, and Gln-66 (Y.-H. Kao, unpublished data). These results correlate well with the disordered regions described above except the region of residues 47−52. This slightly disordered section is probably a result of insufficient NOE constraints in the structure calculation, not the mobility of this region.

*Calcium Binding Affinity of FVII EGF-1.* The $Ca^{2+}$-binding site in FVII EGF-1 is essential for the activity of FVIIa as well as its interaction with sTF (*11*, *12*). To investigate whether the fucosylation affects the $Ca^{2+}$ affinity of FVII EGF-1, we measured the $Ca^{2+}$ dissociation constant for the isolated FVII EGF-1 domain using 1D NMR. A number of individual peaks (e.g., $C^{\gamma}H_2$ of Pro-54 and $H^{\alpha/\delta}$ of Tyr-68) in 1D proton spectra recorded in $D_2O$ are affected by the addition of $CaCl_2$. By following the $^{1}H$ chemical shift of these signals as a function of $CaCl_2$ concentration, the $K_d$ was determined to be 16.4 ± 1.8 and 8.6 ± 1.4 mM for nonfucosylated and fucosylated FVII EGF-1, respectively, in the presence of 150 mM NaCl at pH 7.3 (Figure 8). These results indicate that the fucosylation has a small effect on the $Ca^{2+}$ affinity of the isolated FVII EGF-1. In addition, these $Ca^{2+}$-binding affinities are weaker than those determined for EGF-like domains from blood coagulation factor IX ($K_d$ =1.8 mM) (*59*) and factor X ($K_d \approx$ 2 mM) (*25*, *60*, *61*) using similar methods. The lower $Ca^{2+}$ affinity for FVII EGF-1 is somewhat puzzling since X-ray (*6*, *62*) and NMR (*63*, *64*) studies indicated that the N-terminal EGF-like domains from factors VII, IX, and X have similar $Ca^{2+}$-binding site structures.

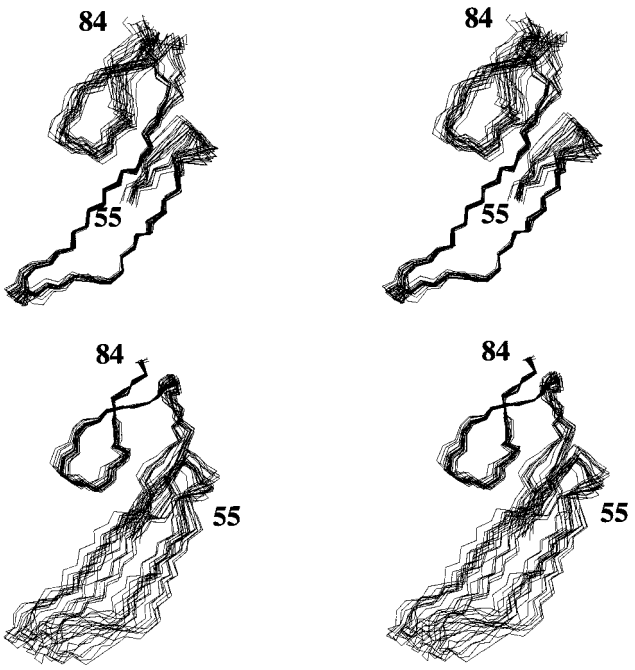


FIGURE 6: Stereoviews showing superposition of the backbone atoms for residues 55−84 in FVII EGF-1. Only the fucosylated structures are displayed, the same views of the nonfucosylated structures are identical. The upper is the best-fit superposition of the first $\beta$-sheet (residues 60−63 and 68−71), and the lower is the best-fit superposition of the second $\beta$-sheet (residues 76−77 and 83−84). For the best fit of the first $\beta$-sheet, the average pairwise rmsd values for the backbone atoms are 0.22 ± 0.08 Å (nonfucosylated) and 0.29 ± 0.08 Å (fucosylated). For the best fit of the second $\beta$-sheet, the average pairwise rmsd values for the backbone atoms are 0.18 ± 0.08 Å (nonfucosylated) and 0.21 ± 0.08 Å (fucosylated).

The weak $Ca^{2+}$-binding affinity measured for the isolated FVII EGF-1 is also inconsistent with the high binding affinity (~150 $\mu$M) reported for the EGF-1 domain in the recombinant FVII and FVII lacking the Gla domain (*65, 66*). It is unclear as to why the individual EGF-1 domain has a much lower $Ca^{2+}$ affinity. However, these observations suggest that residues not directly in contact with the $Ca^{2+}$ must also participate in mediating $Ca^{2+}$ binding. It has been documented that the presence of the Gla domain in factor X significantly increases the $Ca^{2+}$-binding affinity of its EGF-like domain (*61*). In addition, NMR and small-angle X-ray scattering studies on factor X indicated that $Ca^{2+}$ binding brings the Gla domain toward the EGF-1 domain and stabilizes this region of factor X (*14*). Thus, the absence of the Gla domain may be responsible for the reduced $Ca^{2+}$ affinity of the isolated EGF-1 of FX. A similar effect is likely to exist in the isolated FVII EGF-1. In fact, the X-ray structure of FVIIa and sTF complex (*6*) shows that the $Ca^{2+}$-binding site is encompassed by several residues near the Gla domain and the short loop (residues 64−67) connecting the $\beta$-strands I and II. One of the ligands for the $Ca^{2+}$, Asp-46, is located in the very last turn of the helix at the boundary between the Gla and EGF-1 domains. The amide proton of Asp-46 forms a hydrogen bond with Ser-43 O and/or Ile-42 O in the X-ray structure. Thus, the removal of the Gla domain and lack of the helical structure may have a direct impact on the N-terminal structure and the $Ca^{2+}$-binding affinity of FVII EGF-1. This idea is supported by the disorder in residues 45, 46, and 66 as described above and in Muranyi et al. (*13*).

*FVII EGF-1−Tissue Factor Binding Affinity.* EGF-1 domain affinity for sTF was determined from the concentration dependence of inhibition of FVIIa amidolytic activity on the substrate chromozym t-PA. A high $Ca^{2+}$ concentration (50 mM) was used in these experiments to promote saturation of the $Ca^{2+}$-binding site on EGF-1. sTF binding enhances the catalytic efficiency of FVIIa toward chromozym t-PA by about 12-fold at pH 7.5 (*67*). The single EGF-1 domains inhibit the sTF stimulation of FVIIa amidolytic activity with an $IC_{50}$ of 600 ± 500 $\mu$M (nonfucosylated) and 800 ± 800 $\mu$M (fucosylated). These values show that the EGF-1 domains bind only very weakly to sTF. Within the experimental error in these measurements, there is no difference in apparent binding affinity between fucosylated and nonfucosylated EGF-1. The large error in the $IC_{50}$ values reflects the difficulty in measuring weak binding in that it was not practical to use EGF-1 concentrations high enough (>1 mM) to obtain a complete inhibition curve. These affinities are too weak to measure using either surface plasmon resonance methods (*7*) or isothermal titration calorimetry (G. Lee, unpublished results).

The interaction between FVII EGF-1 and sTF, albeit weak, was observed by a series of HSQC spectra of $^{15}N$-labeled FVII EGF-1 recorded in the presence of varying concentrations of TF (data not shown). While no major chemical shift changes were detected for FVII EGF-1 upon binding to sTF, exchange broadening was observed for those residues involved in the binding interface (*6*), indicating a specific interaction with sTF. For example, the HSQC spectrum of FVII EGF-1 recorded in the presence of sTF showed that the cross-peaks of Gly-78, Arg-79, and the side-chain amide signals of Gln-64 were completely unobservable. In addition, the amide peak for Ile-69 was significantly broadened. These residues have been shown to have direct contact with TF in the X-ray structure of FVIIa:sTF complex (*6*). The same perturbations were observed for the fucosylated sample. Except for those residues involved in the calcium-binding site, the signals from residues that do not have direct contact with TF were only slightly broadened. The exchange rate between sTF-bound and free forms is in the intermediate range on the NMR time scale, making it difficult to estimate the binding affinity based solely on HSQC data.

Previous mutagenesis studies of FVII (*9, 68, 69*) have identified several residues within the EGF-1 domain that are essential for the interaction with tissue factor: Gln-64, Ile-69, Phe-71, and Arg-79. These four residues are located on the same side of FVII EGF-1. When complexed with TF, they are in direct contact with residues from TF via hydrogen bonds or hydrophobic interactions (*6*). Among these residues, only the side chains of Phe-71 and Gln-64 are well-defined in the solution structure (Figure 9). Several side-chain NOEs were observed for Ile-69 and included in the structure calculation; however, these NOEs are not sufficient to yield a well-defined side-chain position. The HNHB, 3D $^{1}H$-$^{15}N$ HSQC-TOCSY and short mixing time NOESY data suggest that the $\chi_1$ dihedral angle of Ile-69 is disordered. In the final NMR structures, it is evenly distributed among the 180° and −60° rotamers. In the X-ray structure of FVIIa-sTF complex (*6*), however, the side chain of Ile-69 is in a +60° rotamer. Although Arg-79, located in the $\beta$-turn connecting the two

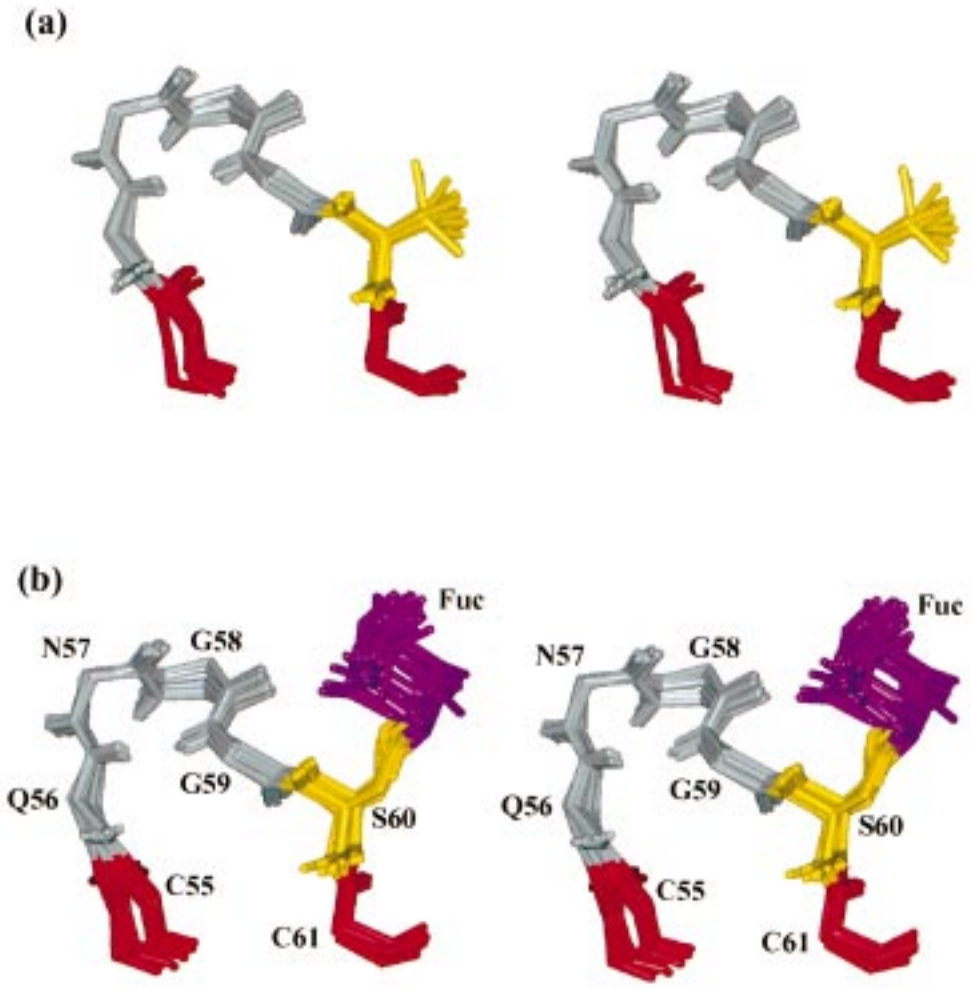


FIGURE 7: Stereoviews showing best-fit superposition of the backbone atoms for residues 55−61: (a) nonfucosylated and (b) fucosylated FVII EGF-1. Residues 55−61 correspond the putative consensus sequence, CXXGG**S/T**C, identified for the fucosylation site in several EGF-like domains (*17*). In both panels a and b, the fucosylation site (Ser-60) is shown in yellow; the type I′ $\beta$-turn (56−59) is shown in gray; and the two flanking Cys residues are shown in red. In panel b, the fucose is shown in purple.

short strands (III and IV), has specific contacts with residues from sTF in the X-ray structure of FVIIa-sTF complex, its long side chain is poorly defined in the NMR structure. This is consistent with a disordered $\chi_1$ rotamer as suggested by the HNHB and 3D $^1$H-$^{15}$N HSQC-TOCSY and NOESY results. The fucosylation again does not alter the conformations of these residues significantly.

The full-length FVIIa binds to sTF with a $K_d$ of approximately 4−6 nM (*7*, *9*). On the basis of mutagenesis experiments on both sTF (*7*) and FVIIa (*9*), the interaction of the EGF-1 domain with TF is estimated to provide about 70% of the free energy of binding for the formation of FVIIa:sTF complex. However, in the absence of the other domains, this interaction is not sufficient to give high-affinity binding. Apparently, cooperative interactions with the other domains of FVIIa are required for EGF-1 to make a large contribution to the free energy of binding. The results presented here are consistent with those reported by Kazama et al. (*70*), who showed that a fragment prepared by proteolysis of human FVIIa, and consisting of the EGF-1 domain and the N-terminus of EGF-2, did not have measurable affinity for tissue factor. In addition, our studies show that the fucosylation of Ser-60 does not influence binding of isolated FVII EGF-1 domain to sTF. However, Iino et al. (*21*) recently reported that alanine mutation at Ser-60 decreases the affinity of the full length FVIIa for TF, based on a reduced association rate constant ($k_{on}$) and an identical dissociation rate constant ($k_{off}$) for TF. This suggests that the mechanism by which the fucose affects the FVIIa:TF interaction must involve domains other than EGF-1.

*Effect of Fucosylation.* As described above, the fucose appears to have no effect on the interaction between the isolated FVII EGF-1 and sTF. However, the removal of the fucosylation site in the full-length FVIIa decreases its affinity for TF (*21*). There are two possible explanations for this observation. The affinity of the isolated FVII EGF-1 for TF may be too weak for the fucose to have a measurable effect. Alternatively, the fucose may influence the interaction between the full-length FVIIa and TF through the Gla domain. Although the fucose and the Gla domain are not in proximity to each other, it is still possible that the fucose can affect the Gla domain via the $Ca^{2+}$-binding site. This idea is supported by the observation that the fucose can influence the $Ca^{2+}$-binding affinity of the isolated FVII EGF-1 (see above). Since the role of the $Ca^{2+}$-binding site in the EGF-1 of FX is believed to alter and stabilize the relative orientation of Gla and EGF-1 domains (*14*), a similar mechanism is likely to exist in FVII and to provide a means

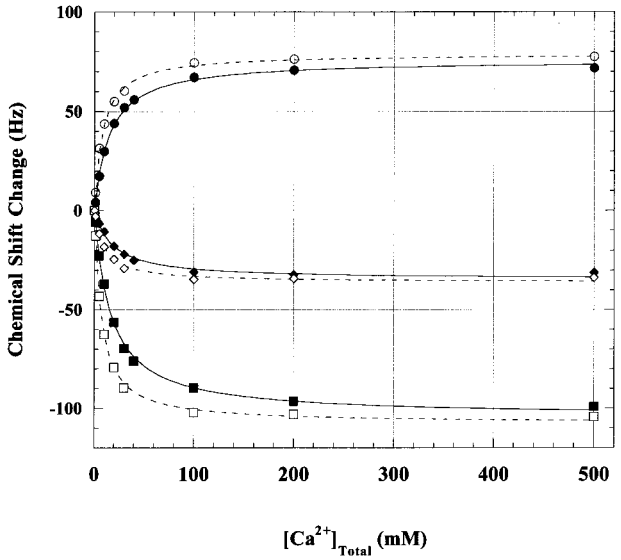


FIGURE 8: The plot of chemical shift change (Hz) of $H^{\alpha}$ [(■) nonfucosylated; (□) fucosylated] and $H^{\delta}$ [(◆) nonfucosylated; (◇) fucosylated] of Tyr-68, and $C^{\gamma}H_2$ [(●) nonfucosylated; (○) fucosylated] of Pro-54 vs total $Ca^{2+}$ concentration in the sample. The titration data were fitted using a single binding site model. The average dissociation constants ($K_d$) of $Ca^{2+}$ determined from these curves are 16.4 ± 1.8 (solid line) and 8.6 ± 1.4 mM (dashed line) for nonfucosylated and fucosylated FVII EGF-1, respectively.

for the fucose to influence the FVII-TF interaction. Furthermore, the presence of fucose at Ser-60 appears to increase the backbone $\phi$ and $\psi$ angular order parameters for residues 64−66. Since the fucose does not have any long-range NOEs to residues 64−66, it is likely that the flexibility of the loop connecting $\beta$-strands I and II may be indirectly limited by the fucose and that the $Ca^{2+}$-binding site might be under the influence of the fucose. Although the effect of the fucosylation on the $Ca^{2+}$-binding affinity is small (only 2-fold), it may be sufficient to influence the function of the $Ca^{2+}$ binding site in FVII EGF-1. It is also possible that the fucosylation may have a much larger effect on the $Ca^{2+}$ affinity when the structural integrity of the $Ca^{2+}$ binding site is maintained by the presence of the Gla domain.

The effect of carbohydrate on the protein conformation is clearly protein dependent (*71*, *72*). For example, Wyss et al. (*73*) reported that removing the mannose residues from the high-mannose type N-glycan in the adhesion domain of human T-cell surface glycoprotein, CD2 ($hsCD2_{105}$), does not significantly affect its CD spectrum; however, the removal of the last sugar residue, GlcNAc, gives rise to a completely different CD spectrum and causes aggregation and destabilization of $hsCD2_{105}$. This suggests that a single sugar residue can have a major impact on the protein conformation and may contribute significantly to the stability of a protein. Conversely, the structural comparison of nonfucosylated and fucosylated proteinase inhibitor, PMP-C, indicated that conformational rearrangement is limited to the vicinity of the fucose (*74*). Similar to the case of PMP-C, the fucose evidently does not cause any significant structural perturbation in FVII EGF-1 domain. There are at least two explanations for this. First, a space is available to accommodate the fucose without introducing steric hindrance. Second, an EGF-like structural motif has a constrained framework formed by the three disulfide bridges; therefore, the attachment of a single fucose on an exposed Ser is unlikely to alter the conformation. The structural perturbation caused by the fucosylation is small, however, as discussed above, subtle changes may still have a significant impact on the function of FVII.

## CONCLUSIONS

In summary, our studies indicate that the isolated FVII EGF-1 domain is insufficient to form a tight complex with sTF. The solution structures of both nonfucosylated and fucosylated FVII EGF-1 were determined by NMR spectroscopy. Both structures are very similar to the FVII EGF-1 domain in the X-ray structure of FVIIa:sTF complex (*6*). The structures of the FVII EGF-1 domain reported up to date are all very similar under various conditions (*6*, *13*, and this work), indicating that the EGF-like domain is a very stable structure motif. The weak affinity of the isolated FVII EGF-1 for TF is thus not due to incorrect folding of the isolated domain. The tight binding affinity of FVIIa for TF

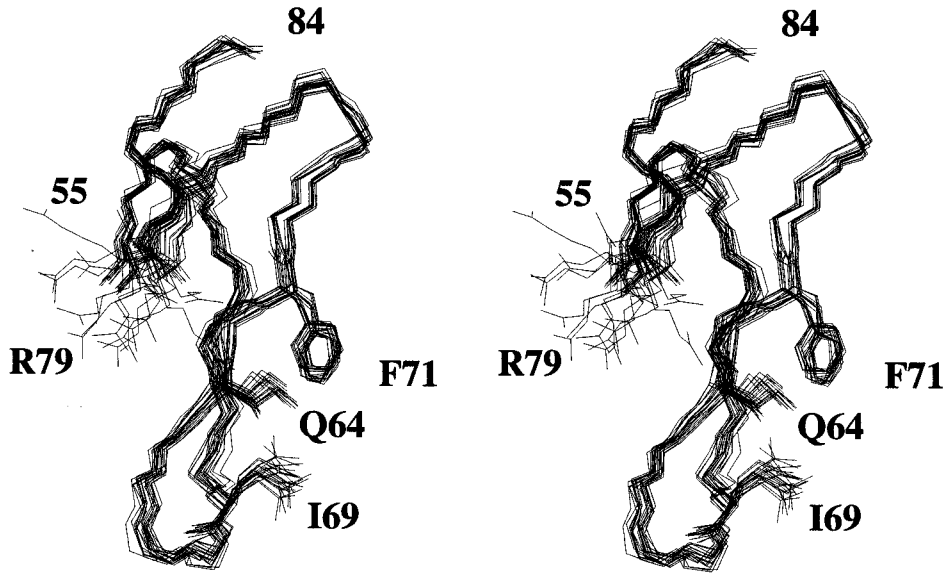


FIGURE 9: Stereoviews showing superposition of the backbone atoms for residues 55−84 in FVII EGF-1. Only the fucosylated structures are displayed, the same views of the nonfucosylated structures are identical. The side-chains of the residues involved in the interaction with tissue factor are shown: Gln-64, Ile-69, Phe-71, and Arg-79.

is most likely a result of cooperative interaction of all four domains in FVII with TF. Fucosylation at Ser-60 has no major effect on the conformation of FVII EGF-1 or its interaction with sTF. However, the presence of fucose appears to slightly increase the $Ca^{2+}$ affinity of the isolated FVII EGF-1. In addition, subtle conformational change upon fucosylation, which is not clearly defined in the NMR structures, may still exist. Since the $Ca^{2+}$ binding is critical to the high affinity complex of FVIIa and TF, it is possible that the fucosylation at Ser-60 stabilizes the $Ca^{2+}$ the binding site in FVIIa and allows the FVIIa to adopt an optimal conformation for the interaction with TF.

## ACKNOWLEDGMENT

We thank Nicholas Skelton, Wayne Fairbrother, and Reed Harris for valuable advice and discussion; Dorothea Reilly for providing $^{15}$N-labeled FVII EGF-1; Mark O'Connell for providing the FVIIa used in TF binding affinity study; Felicity Shen for amino acid analysis of FVII EGF-1; and Damon Papac, Ed Chin, and Long Truong for mass spectrometry analysis.

## SUPPORTING INFORMATION AVAILABLE

Table S1 contains $^{15}$N and $^{1}$H chemical shift assignments. Figure S1 displays a 3D $^{1}$H-$^{15}$N NOESY-HSQC composite strip plots for residues 57−67. Figure S2 compares the schematic representations of the energy-minimized mean structures of nonfucosylated and fucosylated FVII EGF-1. This material is available free of charge via the Internet at http://pubs.acs.org.

## REFERENCES

1. Edgington, T. S., Dickinson, C. D., and Ruf, W. (1997) *Thromb. Haemost. 78*, 401−405.
2. Lee, G. F., Lazarus, R. A., and Kelley, R. F. (1997) *Biochemistry 36*, 5607−5611.
3. Harlos, K., Martin, D. M., O'Brien, D. P., Jones, E. Y., Stuart, D. I., Polikarpov, I., Miller, A., Tuddenham, E. G., and Boys, C. W. (1994) *Nature 370*, 662−666.
4. Muller, Y. A., Ultsch, M. H., Kelley, R. F., and de Vos, A. M. (1994) *Biochemistry 33*, 10864−10870.
5. Muller, Y. A., Ultsch, M. H., and de Vos, A. M. (1996) *J. Mol. Biol. 256*, 144−159.
6. Banner, D. W., D'Arcy, A., Chene, C., Winkler, F. K., Guha, A., Konigsberg, W. H., Nemerson, Y., and Kirchhofer, D. (1996) *Nature 380*, 41−46.
7. Kelley, R. F., Costas, K. E., O'Connell, M. P., and Lazarus, R. A. (1995) *Biochemistry 34*, 10383−10392.
8. Chang, J.-Y., Stafford, D. W., and Straight, D. L. (1995) *Biochemistry 34*, 12227−12232.
9. Dickinson, C. D., Kelly, C. R., and Ruf, W. (1996) *Proc. Natl. Acad. Sci. U.S.A. 93*, 14379−14384.
10. Campbell, I. D., and Bork, P. (1993) *Curr. Opin. Struct. Biol. 3*, 385−392.
11. Kelley, C. R., Dickinson, C. D., and Ruf, W. (1997) *J. Biol. Chem. 28*, 17467−17472.
12. Persson, E., Olsen, O. H., Ostergaard, A., and Nielsen, L. S. (1997) *J. Biol. Chem. 272*, 19919−19924.
13. Muranyi, A., Finn, B. E., Gippert, G. P., Forsén, S., Stenflo, J., and Drakenberg, T. (1998) *Biochemistry 37*, 10605−10615.
14. Sunnerhagen, M., Olah, G. A., Stenflo, J., Forsén, S., Drakenberg, T., and Trewhella, J. (1996) *Biochemistry 35*, 11547−11559.
15. Nishimura, H., Kawabata, S., Kisiel, W., Hase, S., Ikenaka, T., Takao, T., Shimonishi, Y., and Iwanaga, S. (1989) *J. Biol. Chem. 264*, 20320−20325.
16. Bjoern, S., Foster, D. C., Thim, L., Wiberg, F. C., Christensen, M., Komiyama, Y., Pedersen, A. H., and Kisiel, W. (1991) *J. Biol. Chem. 266*, 11051−11057.
17. Harris, J. R., and Spellman, M. W. (1993) *Glycobiology 3*, 219−224.
18. Varki, A. (1993) *Glycobiology 3*, 97−130.
19. Dwek, R. A. (1996) *Chem. Rev. 96*, 683−720.
20. Wyss, D. F., and Wagner, G. (1996) *Curr. Opin. Biotech. 7*, 409−416.
21. Iino, M., Foster, D. C., and Kisiel, W. (1998) *Arch. Biochem. Biophys. 352*, 182−192.
22. Wang, Y., Lee, G. F., Kelley, R. F., and Spellman, M. W. (1996) *Glycobiology 6*, 837−842.
23. Wang, Y., and Spellman, M. W. (1998) *J. Biol. Chem. 273*, 8112−8118.
24. Reilly, D., and Fairbrother, W. J. (1994) *J. Biomol. NMR 4*, 459−462.
25. Persson, E., Selander, M., Linse, S., Drakenberg, T., Ohlin, A. K., and Stenflo, J. (1989) *J. Biol. Chem. 264*, 16897−16904.
26. Kelley, R. F., Refino, C. J., O'Connell, M. P., Modi, N., Sehl, P., Lowe, D., Pater, C., and Bunting, S. (1997) *Blood 89*, 3219−3227.
27. Rance, M., Sorensen, O. W., Bodenhausen, G., Wagner, G., Ernst, R. R., and Wüthrich, K. (1983) *Biochem. Biophys. Res. Commun. 117*, 479−485.
28. Braunschweiler, L., Bodenhausen, G., and Ernst, R. R. (1983) *Mol. Phys. 48*, 535−560.
29. Rance, M., and Wright, P. E. (1986) *J. Magn. Reson. 66*, 372−378.
30. Braunschweiler, L., and Ernst, R. R. (1983) *J. Magn. Reson. 53*, 521−528.
31. Rance, M. (1987) *J. Magn. Reson. 74*, 557−564.
32. Kumar, A., Ernst, R. R., and Wüthrich, K. (1980) *Biochem. Biophys. Res. Commun. 95*, 1−6.
33. Bodenhausen, G., Kogler, H., and Ernst, R. R. (1984) *J. Magn. Reson. 58*, 370−388.
34. Hwang, T.-L., and Shaka, A. J. (1995) *J. Magn. Reson., Ser. A 112*, 275−279.
35. Cavanagh, J., and Rance, M. (1992) *J. Magn. Reson. 96*, 670−678.
36. Drobny, G., Pines, A., Sinton, S., Weitekamp, D. P., and Wemmer, D. (1979) *Symp. Faraday Soc. 13*, 49−55.
37. Marion, D., and Wüthrich, K. (1983) *Biochem. Biophys. Res. Commun. 113*, 967−974.
38. Marion, D., Ikura, M., Tschudin, R., and Bax, A. (1989) *J. Magn. Reson. 85*, 393−399.
39. Grzesiek, S., and Bax, A. (1993) *J. Am. Chem. Soc. 115*, 12593−12594.
40. Zhang, O., Kay, L. E., Olivier, J. P., and Forman-Kay, J. D. (1994) *J. Biomol. NMR 4*, 845−858.
41. Kay, L. E., Keifer, P., and Saarinern, T. (1992) *J. Am. Chem. Soc. 114*, 10663−10665.
42. Muhandiram, D. R., and Kay, L. E. (1994) *J. Magn. Reson. Ser. B 103*, 203-216.
43. Shaka, A. J., Keller, J., and Freeman, R. (1983) *J. Magn. Reson. 53*, 313−340.
44. Shaka, A. J., Barker, P. B., and Freeman, R. (1985) *J. Magn. Reson. 64*, 547−552.
45. Archer, S. J., Ikura, M., Torchia, D. A., and Bax, A. (1991) *J. Magn. Reson. 95*, 636−641.
46. Vuister, G. W., and Bax, A. (1993) *J. Am. Chem. Soc. 115*, 7772−7777.
47. Wagner, G., Braun, W., Havel, T. F., Schaumann, T., Go, N., and Wüthrich, K. (1987) *J. Mol. Biol. 196*, 611−639.
48. Powers, R., Garrett, D. S., March, C. J., Frieden, E. A., Gronenborn, A. M., and Clore, G. M. (1993) *Biochemistry 32*, 6744−6762.
49. Nilges, M., Clore, G. M., and Gronenborn, A. M. (1988) *FEBS Lett. 229*, 317−324.
50. Fletcher, C. M., Harrison, R. A., Lachmann, P. J., and Neuhaus, D. (1994) *Curr. Biol. 2*, 185−199.
51. Brünger, A. T. (1996) *X-PLOR Version 3.851*, copyright 1996 by Yale University.

52. Wüthrich, K. (1986) *NMR of Proteins and Nucleic Acids*, John Wiley and Sons, New York.
53. Laskowski, R. A., Rullmann, J. A. C., MacArthur, M. W., Kaptein, R., and Thornton, J. M. (1996) *J. Biomol. NMR 8*, 477−486.
54. Hyberts, S., Goldberg, M. S., Havel, T. F., and Wagner, G. (1992) *Protein Sci. 1*, 736−751.
55. Li, Y.-C., and Montelione, G. T. (1995) *Biochemistry 34*, 2408−2423.
56. Fairbrother, W. J., Liu, J., Pisacane, P. I., Sliwkowski, M. X., and Palmer, A. G. (1998) *J. Mol. Biol. 279*, 1149−1161.
57. Richardson, J. S. (1981) *Adv. Protein Chem. 34*, 167−339.
58. Wilmot, C. M., and Thornton, J. M. (1988) *J. Mol. Biol. 203*, 221−232.
59. Handford, P. A., Mayhew, M., Baron, M., Winship, P. R., Campbell, I. D., and Brownlee G. G. (1991) *Nature 351*, 317−324.
60. Selander-Sunnerhagen, M., Persson, E., Dahlqvist, I., Drakenberg, T., Stenflo, J., Mayhew, M., Robin, M., Hanford, P., Tilley, J. W., Campbell, I. D., and Brownless, G. G. (1993) *J. Biol. Chem. 268*, 23339−23344.
61. Valcarce, C., Selander-Sunnerhagen, M., Tamlitz, A. M., Drakenberg, T., Bjork, I., and Stenflo J. (1993) *J. Biol. Chem. 268*, 26673−26678.
62. Rao, Z., Handford, P., Mayhew, M., Knott, V., Brownlee, G. G., and Stuart, D. (1995) *Cell 82*, 131−141.
63. Selander-Sunnerhagen, M., Ullner, M., Persson, E., Teleman, O., Stenflo, J., and Drakenberg, T. (1992) *J. Biol. Chem. 267*, 19642−19649.
64. Baron, M., Norman, D. G., Harvey, T. S., Handford, P. A., Mayhew, M., Tse, A. G. D., Brownlee, G. G., and Campbell, I. D. (1992) *Protein Sci. 1*, 81−90.
65. Schiødt, J., Harrit, N., Christensen, U., and Petersen, L. C. (1992) *FEBS Lett. 306*, 265−268.
66. Sabharwal A. K., Birktoft, J. J, Gorka, J., Wildgoose, P., Petersen, L. C., and Bajaj, S. P. (1995) *J. Biol. Chem. 270*, 15523−15530.
67. Neuenschwander, P. F., Branam, D. E., and Morrissey, J. H. (1993) *Thromb. Haemost. 70*, 970−977.
68. Sridhara, S., Clarke, B. J., and Blajchman, M. A. (1993) *Blood Coagulation Fibrinol. 4*, 505−506.
69. O'Brien, D. P., Kemball-Cook, G., Hutchinson, A. M., Martin, D. M., Johnson, D. J., Byfield, P. G., Takamiya, O., Tuddenham, E. G., and McVey, J. H. (1994) *Biochemistry 33*, 14162−14169.
70. Kazama, Y., Pastuszyn, A., Wildgoose, P., Hamamoto, T., and Kisiel, W. (1993) *J. Biol. Chem. 268*, 16231−16240.
71. Goochee, C. F., Gramer, M. J., Anderson, D. C., and Bahr, J. B. (1992) *Frontiers in Bioprocessing II*, pp 199−240, American Chemical Society, Washington, DC.
72. Lis, H., and Sharon, N. (1993) *Eur. J. Biochem. 218*, 1−27.
73. Wyss, D. F., Choi J. S., Li, J., Knoppers, M. H., Willis, K. J., Arulanandam, A. R., Smolyar, A., Reinherz, E. L., and Wagner, G. (1995) *Science 269*, 1273−1278.
74. Mer, G., Hietter, H., and Lefevre, J. F. (1996) *Nat. Struct. Biol. 3*, 45−53.

BI990234Z